The Astrophysical Journal Letters, 885:L38 (5pp), 2019 November 10 https://doi.org/10.3847/2041-8213/ab5193

Constraining X-Ray Coronal Size with Transverse Motion of AGN Ultra-fast Outflows

Keigo Fukumura[1] and Francesco Tombesi[2,3,4,5]
[1] Department of Physics and Astronomy, James Madison University, Harrisonburg, VA 22807, USA; fukumukx@jmu.edu
[2] Astrophysics Science Division, NASA/Goddard Space Flight Center, Greenbelt, MD 20771, USA
[3] Department of Astronomy, University of Maryland, College Park, MD 20742, USA
[4] Department of Physics, University of Rome "Tor Vergata," Via della Ricerca Scientifica 1, I-00133 Rome, Italy
[5] INAF Astronomical Observatory of Rome, Via Frascati 33, I-00078 Monteporzio Catone (Rome), Italy
Received 2019 October 2; revised 2019 October 21; accepted 2019 October 28; published 2019 November 8

Abstract

One of the canonical physical properties of ultra-fast outflows (UFOs) seen in a diverse population of active galactic nuclei is its seemingly very broad width (i.e., $\Delta v \gtrsim 10{,}000$ km s^{-1}), a feature often required for X-ray spectral modeling. While unclear to date, this condition is occasionally interpreted and justified as internal turbulence within the UFOs for simplicity. In this work, we exploit a transverse motion of a three-dimensional accretion disk-wind, an essential feature of nonradial outflow morphology unique to magnetohydrodynamic outflows. We argue that at least part of the observed line width of UFOs may reflect the degree of transverse velocity gradient due to Doppler broadening around a putative compact X-ray corona in the proximity of a black hole. In this scenario, line broadening is sensitive to the geometrical size of the corona, R_c. We calculate the broadening factor as a function of coronal radius R_c and velocity smearing factor $f_{\rm sm}$ at a given plasma position. We demonstrate, as a case study of the quasar, PDS 456, that the spectral analysis favors a compact coronal size of $R_c/R_g \lesssim 10$ where R_g is gravitational radius. Such a compact corona is long speculated from both an X-ray reverberation study and the lamppost model for disk emission also consistent with microlensing results. Combination of such a transverse broadening around a small corona can be a direct probe of a substantial rotational motion perhaps posing a serious challenge to radiation-driven wind viewpoint.

Unified Astronomy Thesaurus concepts: Black hole physics (159); High energy astrophysics (739); Radiative processes (2071); Seyfert galaxies (1447); X-ray active galactic nuclei (2035); Accretion (14); Magnetohydrodynamics (1964)

1. Introduction

Ultra-fast outflows (UFOs) are an intriguing subclass of ionized outflows in the form of resonant absorption lines seen primarily by high-throughput CCD observations in about 40% of active galactic nuclei (AGNs; Tombesi et al. 2010, 2014, 2015; Gofford et al. 2013) including very bright (lensed) quasars (QSOs; Chartas et al. 2003, 2009; Pounds et al. 2003; Reeves et al. 2003, 2018; Lanzuisi et al. 2012; Vignali et al. 2015; Dadina et al. 2018). They are detected also in non-AGN sources such as ultra-luminous X-ray sources (Walton et al. 2016) and potentially tidal disruption events (e.g., Kara et al. 2018). In general, canonical X-ray UFOs[6] are known to exhibit extreme physical conditions, namely, a massive column density ($N_H \gtrsim 10^{23}$ cm^{-2}), highly ionized state (of ionization parameter[7] of $\log \xi \sim 4$–6) outflowing at near-relativistic speed ($v/c \sim 0.1$–0.7). Because of its energetically powerful nature, UFOs can be good candidates to effectively deliver a sufficient amount of energy and momentum out to host galaxies at ∼kiloparsec scale to quench star formation activity (e.g., Hopkins & Elvis 2010; Tombesi et al. 2015).

Quasar outflows generally have been thought to be driven by radiation pressure by their intense O/UV flux, in a manner similar to that observed in massive stars (King & Pounds 2015; Hagino et al. 2017; Nomura & Ohsuga 2017). On the other hand, most UFOs are highly ionized such that little UV or soft X-ray opacity may be left in the wind, making this process very inefficient (e.g., Higginbottom et al. 2014). In addition, the production region of line-driven UFOs seems to be spatially limited to a very narrow latitudinal region (e.g., $70^\circ \lesssim \theta \lesssim 80^\circ$) according to hydrodynamic simulations (e.g., Nomura & Ohsuga 2017), which casts a doubt in viability with observations. Also, a number of UFOs have been found in sub-Eddington accretors (e.g., Marinucci et al. 2018). To overcome these potential issues, another plausible mechanism —magnetically driven disk-winds—has been proposed to provide an alternative means to efficiently accelerate the highly ionized absorbers as observed (e.g., Blandford & Payne 1982, hereafter BP82; Contopoulos & Lovelace 1994, hereafter CL94; Königl & Kartje 1994; Ferreira 1997; Fukumura et al. 2010, hereafter F10; Kazanas et al. 2012; Kraemer et al. 2018; Kazanas 2019; Fukumura et al. 2018, hereafter F18) in the context of both AGNs and X-ray binaries. Magnetohydrodynamic (MHD) wind in general is thus immune to these issues.

Another puzzle associated with the canonical UFOs is its remarkably broad line width (e.g., $\sigma_{\rm tur} \sim 10{,}000$–$20{,}000$ km s^{-1}) often required for photoionization modeling, for example, with `xstar` that employs an arbitrary choice of internal turbulence parameter (aka `vturb`; e.g., Nardini et al. 2015, hereafter N15; Tombesi et al. 2015; Reeves et al. 2018). Although broadening is phenomenologically interpreted as turbulence presumably intrinsic to the outflowing plasma, such a large velocity dispersion is not easily conceivable from first principle. More specifically, wind morphology would be

[6] Note also that there have been a handful reports implying noncanonical UFOs with low ionization state ($\log \xi \sim 0$–2) and/or low column density ($N_H \sim 10^{20}$–10^{22} cm^{-2}), but this is beyond the scope of the present work (e.g., Gupta et al. 2013; Longinotti et al. 2015; Serafinelli et al. 2019).

[7] This is defined as $\xi \equiv L_{\rm ion}/(nr^2)$ where $L_{\rm ion}$ is ionizing (X-ray) luminosity and n is plasma number density at distance r from the BH.

essentially one-dimensional (i.e., radial) in the context of a radiation-driven scenario, which would leave little room for causing velocity gradient, thus necessarily attributed to something like turbulence. On the other hand, it is more realistic to consider that the broadening might represent the actual wind kinematic field. In F18, for example, line broadening is naturally determined by radial velocity shear (Δv_r) of the wind along a line of sight (LoS) without using `vturb`. Alternatively, magnetically launched winds are known to possess a substantial azimuthal velocity component, v_ϕ, originating from the accretion disk surface (see BP82; CL94; F10). This unique MHD-wind feature has prompted us to exploit the role of the transverse motion in characterizing the UFO spectrum in this Letter.

PDS 456 is a well-studied nearby ($z = 0.184$), radio-quiet QSO hosting a black hole (BH) of mass $M \sim 10^9\ M_\odot$ (e.g., Reeves et al. 2009), being the most luminous AGN in the local universe with a bolometric luminosity of $L_{\rm bol} \sim 10^{47}$ erg s^{-1}. It is among the best-known QSOs to exhibit archetypal UFO signatures in the Fe K band from the past X-ray observations with *Suzaku* (e.g., Reeves et al. 2009; Gofford et al. 2014; Matzeu et al. 2017, hereafter M17), *XMM-Newton*/EPIC, and *NuSTAR* (Behar et al. e.g., 2010; N15) since its first discovery (e.g., Reeves et al. 2003). Extensive spectral analyses so far have systematically revealed the existence of highly ionized UFOs of $v/c \sim 0.2$–0.3 identified as the 1s–2p resonance transitions of Fe XXVI with $N_H \lesssim 10^{24}\,{\rm cm}^{-2}$ and the high ionization parameter of $\log \xi \sim 4$–6 where the detected UFOs may well be located in close proximity to the BH within $\sim 100 R_g$ (e.g., Reeves et al. 2009). Recently, even a faster UFO component has been reported in PDS 456 (e.g., Reeves et al. 2018; Boissay-Malaquin et al. 2019).

Motivated by these observations and ideas, we attribute the line width in this Letter to a significant transverse motion naturally expected in the MHD-wind framework that we have developed earlier. We show how line broadening is dependent on the size of the corona in this model. In Section 2, we overview a physical setup of the problem by introducing the magnetically launched disk-wind model. In Section 3, we present our calculations and the best-fit result of PDS 456 in an attempt to constrain the size of the ionizing X-ray corona. Finally in Section 4, we conclude with a summary and discussion.

2. Model Description

2.1. Magnetized Winds

Considering pure magnetic $\boldsymbol{J} \times \boldsymbol{B}$ force, both magnetic pressure primarily from toroidal field $\propto \vec{\nabla} \boldsymbol{B}^2$ as well as tension due to $(\boldsymbol{B} \cdot \vec{\nabla})\boldsymbol{B}$ can successfully drive a UFO of massive column with the observed relativistic speed being photoionized to have high ξ values (see F10 and F18, and references therein, for more detailed model description).

We employ the self-similar prescription in the radial direction assuming the escaping velocity profile of $v(r, \theta) \propto r^{-1/2} f(\theta)$, where $f(\theta)$ denotes the angular dependence to be calculated and the poloidal field structure is determined by numerically solving the MHD Grad-Shafranov equation as is originally formulated in CL94 and applied in F10.

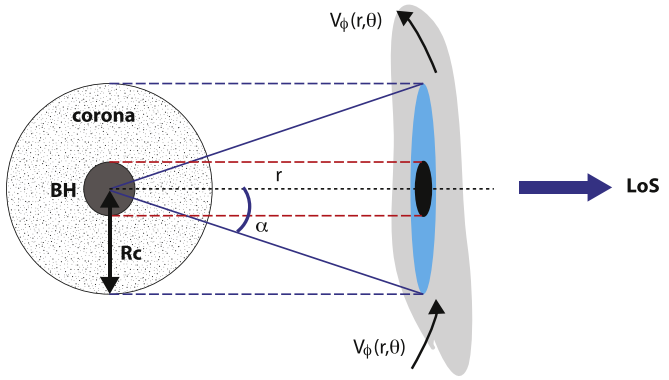

Figure 1. Face-on schematic picture illustrating a transverse wind motion of the plasma (blue region) around a BH corona intersecting a line of sight of a distant observer.

2.2. Line Broadening due to Transverse Motion

The plasma is initially differentially rotating in the disk around a BH in proximity to a putative X-ray corona responsible for photoionizing the surrounding materials. That is, the wind is initially transversing in front of the central corona with respect to a distant observer under axisymmetry, $v_\phi(r, \theta)$. Then, the change in v_ϕ is further dependent on the physical size of the corona near the BH. Consequently, line broadening due to transverse motion in this picture is determined by the coronal size. To quantify the degree of broadening factor, we construct a simplistic toy model, as illustrated in Figure 1, in an attempt to further calculate the effect on the UFO line spectrum. The central corona is assumed to be a spherical region of radius R_c surrounding the BH. While winds are being photoionized isotropically by the corona, classical Doppler shift in velocity depends primarily on (1) the cross-sectional size of the corona, R_c, that intersects with an LoS of a distant observer and (2) the absorber's distance, r.

If the line width is primarily attributed to the transverse motion of the wind under illumination directly in front of the corona (blue region), then the classical azimuthal Doppler shift Δv is expressed by

$$\frac{\Delta v(r, \theta, \phi)}{v_c} \equiv \frac{\boldsymbol{v}_w \cdot \boldsymbol{n}}{c} = \frac{v_\phi(r, \theta; r_o)}{c} \sin\theta_{\rm obs} \sin\phi, \quad (1)$$

where $\boldsymbol{n}$ is a unit vector along an LoS in the spherical coordinates (r, θ, ϕ), $\boldsymbol{r}_o$ is a characteristic innermost launching radius, and v_c denotes a centroid (unmodulated) LoS velocity. Note that the shift due to the poloidal velocity component, $v_p \hat{n_p}$, produces no modulation and thus is ignored here.

Considering that the observed line broadening of UFOs is reflecting the background irradiating coronal size (i.e., radius) as depicted in Figure 1, the solid angle subtended from the center of the corona by the wind plasma at radius r (corresponding to the blue region) yields a relation between the radius R_c and the toroidal angle α such that

$$-\frac{R_c}{r} \leqslant \alpha \leqslant \frac{R_c}{r}. \quad (2)$$

Therefore, by substituting α into ϕ, we note that $\Delta v_i = \Delta v(r, \theta, \phi_i; r_o, R_c)$, where $-\alpha \lesssim \phi_i \lesssim \alpha$ is the ith azimuthal position of the discretized wind. We then calculate its rms

value

$$\Delta v_{\rm rms} = \sqrt{\sum_{i}^{N} (\Delta v_i)^2 / N_\phi} \quad (3)$$

for a characteristic transverse modulation that dictates the line broadening where N_ϕ is the discrete number of the azimuthal plasma position within the angle α. To further accommodate an external smearing effect in transverse motion, we parameterize the effective broadening by introducing a smearing factor $f_{\rm sm}$ as $\Delta v_{\rm eff} \equiv f_{\rm sm}\, \Delta v_{\rm rms}$, where $0.1 \lesssim f_{\rm sm} \lesssim 1$ is assumed.

2.3. Spectral Modeling of Fe K UFOs in PDS 456

We apply the model described above to the simultaneous observations of PDS 456 with *XMM-Newton* and *NuSTAR* in 2013/2014 (see, e.g., N15 and F18). Our current approach directly follows the methodology adopted in F18. For photoionization calculations with `xstar` (Kallman & Bautista 2001), we use the same library of MHD-wind solutions as used in F18 assuming a double broken power-law ionizing spectrum. The local ionic column $N_{\rm ion}$ is computed with `xstar` under thermal equilibrium, while the photoabsorption cross section $\sigma_{\rm abs}$ is calculated using the usual Voigt profile as a function of photon frequency ν and the line-broadening factor $\Delta\nu_\ell \approx (\Delta v_{\rm eff}/c)\nu_c$ relative to the centroid (rest-frame) frequency ν_c. In F18, the line broadening was attributed to the LoS (radial) shear velocity of the wind Δv_r. In this Letter, however, we consider that the transverse (toroidal) motion of the wind primarily contributes to line broadening, as described in Section 2.1. One can then calculate the line optical depth $\tau_\ell = \sigma_{\rm abs} N_{\rm ion}$ to simulate the spectrum. To reduce the degree of freedom in the problem, we adopt some of the model parameters obtained from F18, i.e., LoS angle of $\theta = 50^\circ$ with the X-ray luminosity of $L_{\rm ion} \sim 5 \times 10^{44}$ erg s^{-1} in this specific epoch (see also Gofford et al. 2014; N15; M17) for the wind density profile of $n \propto r^{-1.2}$, although the last assumption is less relevant for the current UFO modeling. Thus, our model in this work has three free parameters that essentially govern the predicted spectrum: density n_{10} in units of 10^{10} [cm^{-3}] of the wind at the innermost launching radius, radius of the corona R_c, and smearing factor $f_{\rm sm}$.

3. Results

3.1. Dependences of Coronal Size

By calculating the broadening effect due to the toroidal motion as a function of R_c, we first calculate the distribution of $\Delta v_{\rm eff}$ as a function of R_c and the wind position r for a given LoS (set to be 50° here as treated in F18). A global morphology of the calculated MHD disk-wind is presented in Figure 2(a) showing its normalized wind density $n(r, \theta)$ and ionization parameter $\xi(r, \theta)$ roughly ranging over 6 orders of magnitudes. Among the generic features of the MHD-wind is dominant toroidal rotation near the launching radius, which is then quickly transformed into poloidal motion as the wind becomes accelerated. It is calculated that the wind possesses a significant transverse motion especially at small radii r, which in our current work is responsible for line broadening. Note that the wind in this domain (i.e., $r/R_g \lesssim 100$) is highly ionized at a high velocity that is important for UFOs.

Being emphasized on the toroidal motion, in Figure 2(b) we also calculate the distribution of the line energy shift due to $\Delta v_{\rm rms}$ determined by Equation (3) as a function of R_c and wind radius r. For $\theta = 50^\circ$ as considered here and in F18, the maximum broadening can be up to $\Delta v_{\rm rms}/c \lesssim 0.1$ for $10 \lesssim r/R_g \lesssim 100$ if $f_{\rm sm} = 1$, which is sufficient to account for the observed line width seen in PDS 456. As R_c increases, a larger fraction of the wind with a wider opening angle comes into the LoS of a distant observer. Hence, $\Delta v_{\rm rms}$ increases with R_c gradually at a given radius r. On the other hand, the toroidal velocity declines with increasing radius as $v_\phi \propto r^{-1/2}$ for a given coronal size. Given the expected distribution of the broadening factor as shown here, one can calculate the line spectrum as discussed in Section 3.2.

3.2. Spectral Fit to Fe K UFOs in PDS 456

Following the same analysis step discussed in F18, we proceed to construct a grid of model spectra with a focus on Fe XXVI in this work. Based on the results obtained in F18, we adopt the earlier derived best-fit value of $R_T \simeq 8$. With χ^2 statistics, we find that the best-fit spectrum model is described by a single power law of photon index $\Gamma = 2.12^{+0.01}_{-0.008}$ supplemented independently by the P-Cygni feature (see N15 and F18) in the form of a Gaussian emission at energy of $E_{\rm P\text{-}Cygni} = 6.43^{+0.22}_{-0.23}$ keV, and the absorption component is well reproduced by our MHD model. We have adopted the galactic absorption using `tbabs` where $N_H^{\rm Gal} = 2.4 \times 10^{21}\,{\rm cm}^{-2}$ (Kalberla et al. 2005). The similarly modeled Lyβ line exhibits insignificant signature due to its lower oscillator strength as expected.

We obtained the best-fit model of $n_{10} = 17.3^{+2.7}_{-6.1}$, $R_c/R_g = 2.63^{+10.9}_{-0.53}$ and $f_{\rm sm} = 0.76^{+0.24}_{-0.48}$ yielding χ^2/dof of 369.69/429 (see Table 1). In Figure 3(a) we show the best-fit spectrum in comparison with data for various parameters. It is inferred that small coronal size (i.e., $R_c/R_g \lesssim 10$) is clearly favored by data, while the smearing factor $f_{\rm sm}$ must accordingly vary. The larger the coronal size, the larger the toroidal motion contribution tends to be. For this reason, the smearing factor needs to be more significant to suppress unnecessarily large line broadening when the corona is relatively large. Last, we have alternatively relaxed the parameter values for both the continuum and the P-Cygni emission line components, and the end result is found to be only weakly sensitive to those parameters. Our spectral modeling thus strongly favors a compact coronal region responsible for photoionization if the line broadening is indeed associated with the wind's transverse motion as considered here.

3.3. Constraint on Coronal Size and Wind's Transverse Motion

As illustrated in Figure 1, the larger the coronal region, the more the line broadening in the spectrum due to the transverse motion. The line, however, would be too broad when the corona is too large, as implied in this work. For the gradient of $v_\phi(r, \theta)$ over a finite angle subtended by the illuminated wind at radius r, we have parameterized the effective velocity width $\Delta v_{\rm eff}$ by introducing the smearing factor $f_{\rm sm}$ satisfying $0.1 \lesssim f_{\rm sm} \lesssim 1$ as described in Section 2.2. In the context of the present UFO model, a large corona that is radially extended beyond $R_c/R_g \gtrsim 10$ is not consistent with the observed UFO width (see Figure 3(b)) regardless of the smearing factor. We have found in F18 that the disk is favored to be truncated at $r/R_g \simeq 16$ to achieve the best-fit spectrum for the same data,

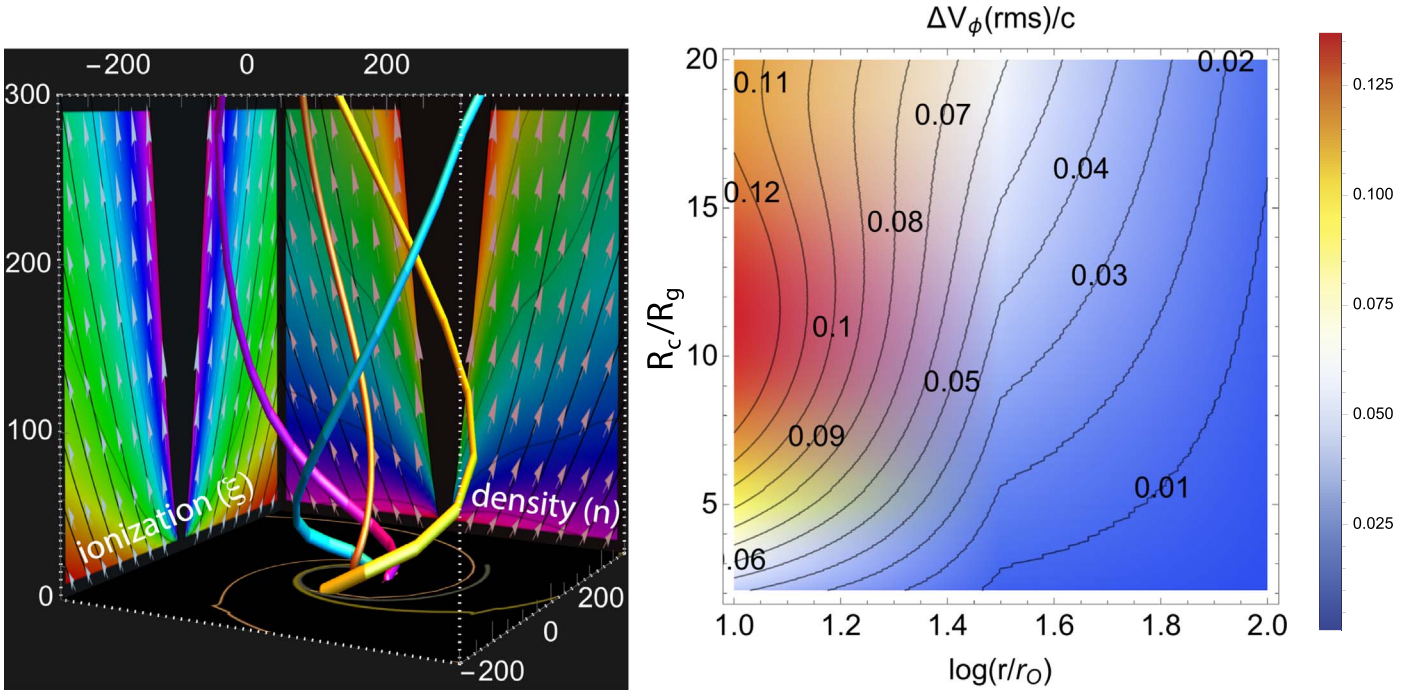

Figure 2. (a) Three-dimensional rendering of the streamlines of fiducial MHD-driven disk-winds considered for the spectral modeling. Normalized wind density $n(r, \theta)$ and ionization parameter $\xi(r, \theta)$ are shown where magenta/dark blue denotes the highest value and yellow/red shows the lowest values (roughly ranging over 6 orders of magnitudes). Transverse motion, especially at small radii, is one of the generic features of the MHD winds. (b) Transverse Doppler broadening factor $\Delta v_{\rm rms}/c$ calculated from a fiducial wind solution (from F18) as a function of LoS radial position r and radial coronal extent R_c for $\theta_{\rm obs} = 50°$.

Table 1
Model Parameters of the MHD-wind

Primary Parameter	Range to Be Considered	Best-fit Value
Power-law photon index Γ	⋯	$2.12^{+0.01}_{-0.008}$ [a]
$E_{\rm P\text{-}Cygni}$ [keV]	⋯	$6.43^{+0.22}_{-0.24}$ [a]
Wind density[b] at the foot point n_{10}	0.01–40	$17.3^{+2.7}_{-6.1}$
R_c/R_g	2–16	$2.63^{+10.9}_{-0.53}$
Smearing factor $f_{\rm sm}$	0.1–1.0	$0.76^{+0.24}_{-0.48}$
χ^2/dof	⋯	369.69/429

Notes. We assume $M = 10^9\ M_\odot$ (Reeves et al. 2009), $\theta_{\rm obs} = 50°$, and $p = 1.2$ (from F18).
[a] Fixed.
[b] Wind density normalization at the launching site in units of 10^{10} cm^{-3}.

which is indeed consistent with the present modeling implying a compact corona of $R_c/R_g \lesssim 10$.

4. Summary and Discussion

We have revisited the archetypal Fe K UFOs observed in PDS 456 in an attempt to account for the broad line width that is usually attributed to internal turbulence in the wind. We adopted the same template spectral models in the MHD accretion disk-wind scenario used in F18 by further exploiting the generic feature of the MHD-driven disk-winds, i.e., substantial transverse motion around a central corona. In this view, we incorporated toroidal rotation of the wind over a finite angle subtended from a compact corona at the location of the plasma. Therefore, the size of the corona determines the modulation of the toroidal velocity of the wind that is under direct coronal illumination (see the blue region in Figure 1). The velocity dispersion in turn contributes to broadening the absorption line. In this Letter, we thus link the line width to the wind's rotation, which is related to the coronal size, thus the UFO line width is used as a proxy to measure the size of the compact corona around the central BH. Note that the coronal geometry should affect little in photoionization and kinematics of the UFOs since it is practically pointlike compared to the distance where Fe XXV/Fe XXVI are formed.

We have demonstrated by spectral modeling of the 2013/2014 *XMM-Newton/NuSTAR* data that the observed Fe XXVI UFO line width of PDS 456 can be potentially used as a measure to infer the central coronal size using the transverse motion within the framework of the magnetically driven disk-winds. Following our earlier spectral modeling in F18, the present model strongly implies a compact corona of a radius of $R_c/R_g \lesssim 10$ with the transverse velocity shift in the wind $\Delta v_{\rm eff}(r) \simeq 0.76\Delta v_{\rm rms}(r)$ (see Table 1 and Figure 3). As a unique feature of the MHD winds, the toroidal motion can be substantial especially at smaller radii around the BH as a distinct property compared with the other driving mechanisms. Our modeling suggests that a corona of only a few gravitational radii is large enough to broaden the line up to what has been observed. The current spectral modeling, an extension from F18, has indicated that the wind's rotational motion can indeed account for the broad line width.

It has been reported by observations of microlensed QSOs that the X-ray-emitting (coronal) region in QSOs is indeed compact ($r/R_g \lesssim 10$; e.g., Morgan et al. 2008; MacLeod et al. 2015; Chartas et al. 2017), consistent with our result. More specifically, the observed broad iron lines of Seyfert 1 s seem to require a very steep emissivity (e.g., $\epsilon \propto r^{-6}$) perhaps indicating a compact hard X-ray source as in coronae (e.g., Fukumura & Kazanas 2007; Wilkins & Fabian 2012; Dauser et al. 2013), while the observed disk reflection component also

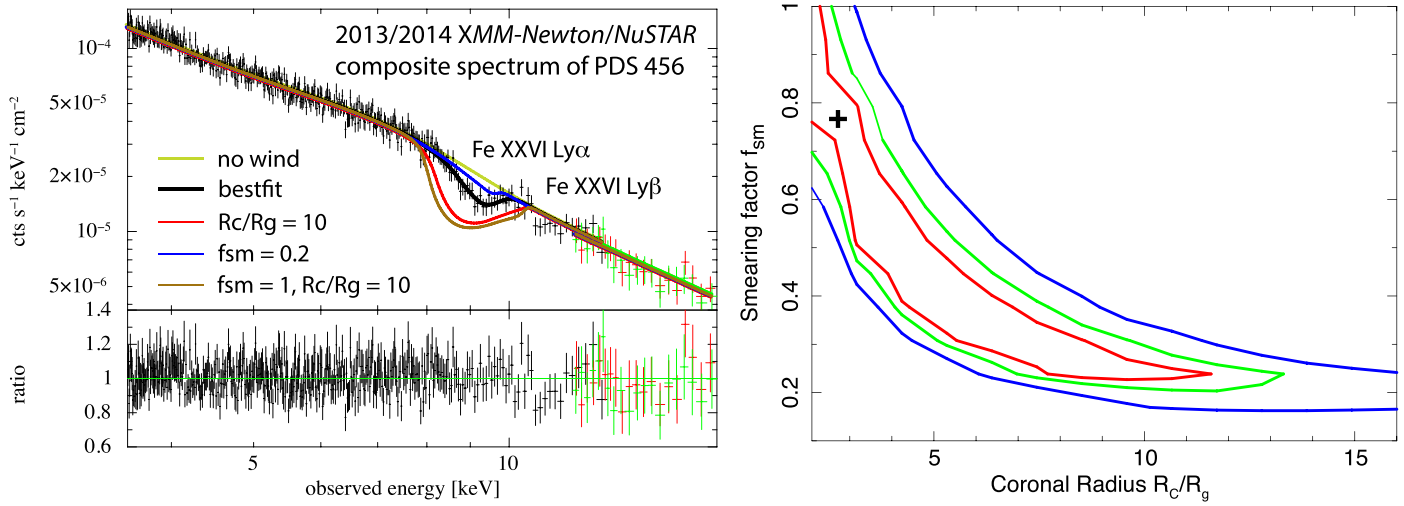

Figure 3. (a) Composite *XMM-Newton*/EPIC-pn/mos (black) and *NuSTAR* (red and green) spectrum of PDS 456 for different model parameters; $R_c/R_g = 10$ (red), best-fit model (dark), $f_{sm} = 1$ (brown), $f_{sm} = 0.2$ (blue), and no wind case (green). (b) Contour map for the coronal radius R_c and smearing factor f_{sm} (confidence levels at 68% in red, 90% in green, and 99% in blue) clearly favoring a compact coronal region with $R_c/R_g \lesssim 10$.

often requires a small-scale "lamppost" corona (e.g., Garcia et al. 2014). These observations and modeling hence necessarily point independently to compactness of a coronal region near the central BH. The property of AGN coronae has been studied explicitly with *NuSTAR* data by constraining the high-energy cutoff in the hard X-ray continuum, independently suggesting a small coronal size (e.g., $r/R_g \sim 3$–10) for a number of AGNs (e.g., Fabian et al. 2015; Kamraj et al. 2018).

Despite intensive theoretical efforts in the past years to better understand the fundamental role of a global magnetic field in the context of BH accretion and outflows, there has been a lack of information from spectral modeling in order to securely disentangle various wind driving mechanisms. More detailed spectral structures can be revealed by the prospective future X-ray missions, such as *XRISM* and *Athena*, which will further help probe the width and ionization structure of the outflows, possibly exploiting absorption line spectroscopy as a technique to map the innermost regions in AGNs.

We are grateful to the anonymous referee for the constructive comments. This work is supported in part by *Chandra* AO-20 archival proposal grants.

ORCID iDs

Keigo Fukumura https://orcid.org/0000-0001-5709-7606

References

Behar, E., Kaspi, S., Reeves, J., et al. 2010, ApJ, 712, 26
Blandford, R. D., & Payne, D. G. 1982, MNRAS, 199, 883, (BP82)
Boissay-Malaquin, R., Danehkar, A., Marshall, H. L., & Nowak, M. A. 2019, ApJ, 873, 29
Chartas, G., Brandt, W. N., & Gallagher, S. C. 2003, ApJ, 595, 85
Chartas, G., Krawczynski, H., Zalesky, L., et al. 2017, ApJ, 837, 26
Chartas, G., Saez, C., Brandt, W. N., Giustini, M., & Garmire, G. P. 2009, ApJ, 706, 644
Contopoulos, J., & Lovelace, R. V. E. 1994, ApJ, 429, 139, (CL94)
Dadina, M., Vignali, C., Cappi, M., et al. 2018, A&A, 610, 13
Dauser, T., Garcia, J., Wilms, J., et al. 2013, MNRAS, 430, 1694
Fabian, A. C., Lohfink, A., Kara, E., et al. 2015, MNRAS, 451, 4375
Ferreira, J. 1997, A&A, 319, 340
Fukumura, K., & Kazanas, D. 2007, ApJ, 664, 14
Fukumura, K., Kazanas, D., Contopoulos, I., & Behar, E. 2010, ApJ, 715, 636, (F10)
Fukumura, K., Kazanas, D., Shrader, C., et al. 2018, ApJL, 864, L27, (F18)
Garcia, J., Dauser, T., Lohfink, A., et al. 2014, ApJ, 782, 76
Gofford, J., Reeves, J. N., Braito, V., et al. 2014, ApJ, 784, 77
Gofford, J., Reeves, J. N., Tombesi, F., et al. 2013, MNRAS, 430, 60
Gupta, A., Mathur, S., Krongold, Y., & Nicastro, F. 2013, ApJ, 772, 66
Hagino, K., Done, C., Odaka, H., Watanabe, S., & Takahashi, T. 2017, MNRAS, 468, 1442
Higginbottom, N., Proga, D., Knigge, C., et al. 2014, ApJ, 789, 19
Hopkins, P. F., & Elvis, M. 2010, MNRAS, 401, 7
Kalberla, P. M. W., Burton, W. B., Hartmann, D., et al. 2005, A&A, 440, 775
Kallman, T., & Bautista, M. 2001, ApJS, 133, 221
Kamraj, N., Harrison, F. A., Balokovic, M., Lohfink, A., & Brightman, M. 2018, ApJ, 866, 124
Kara, E., Dai, L., Reynolds, C. S., & Kallman, T. 2018, MNRAS, 474, 3593
Kazanas, D. 2019, Galax, 7, 13
Kazanas, D., Fukumura, K., Contopoulos, I., Behar, E., & Shrader, C. R. 2012, AstRv, 7, 92
King, A., & Pounds, K. 2015, ARA&A, 53, 115
Köngl, A., & Kartje, J. F. 1994, ApJ, 434, 446
Kraemer, S. B., Tombesi, F., & Bottorff, M. C. 2018, ApJ, 852, 35
Lanzuisi, G., Giustini, M., Cappi, M., et al. 2012, A&A, 544, 2
Longinotti, A. L., Krongold, Y., Guainazzi, M., et al. 2015, ApJ, 813, 39
MacLeod, C. L., Morgan, C. W., Mosquera, A., et al. 2015, ApJ, 806, 258
Marinucci, A., Bianchi, S., Braito, V., et al. 2018, MNRAS, 478, 5638
Matzeu, G. A., Reeves, J. N., Braito, V., et al. 2017, MNRAS, 472, 15, (M17)
Morgan, C. W., Kochanek, C. S., Dai, X., Morgan, N. D., & Falco, E. E. 2008, ApJ, 689, 755
Nardini, E., Reeves, J. N., Gofford, J., et al. 2015, Sci, 347, 860, (N15)
Nomura, M., & Ohsuga, K. 2017, MNRAS, 465, 2873
Pounds, K. A., Reeves, J. N., King, A. R., et al. 2003, MNRAS, 345, 705
Reeves, J. N., Braito, V., Nardini, E., et al. 2018, ApJL, 854, L8
Reeves, J. N., O'Brien, P. T., Braito, V., et al. 2009, ApJ, 701, 493
Reeves, J. N., O'Brien, P. T., & Ward, M. J. 2003, ApJ, 593, 65
Serafinelli, R., Tombesi, F., Vagnetti, F., et al. 2019, A&A, 627, 121
Tombesi, F., Cappi, M., Reeves, J. N., et al. 2010, A&A, 521, 57
Tombesi, F., Meléndez, M., Veilleux, S., et al. 2015, Natur, 519, 436
Tombesi, F., Tazaki, F., Mushotzky, R. F., et al. 2014, MNRAS, 443, 2154
Vignali, C., Iwasawa, K., Comastri, A., et al. 2015, A&A, 583, 141
Walton, D. J., Middleton, M. J., Pinto, C., et al. 2016, ApJL, 826, L26
Wilkins, D. R., & Fabian, A. C. 2012, MNRAS, 424, 1284